Microporous and Mesoporous Materials 357 (2023) 112630

Contents lists available at ScienceDirect

Microporous and Mesoporous Materials

journal homepage: www.elsevier.com/locate/micromeso

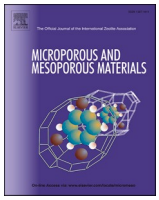

Feasible ethylene separation from a ternary mixture using zeolite-like metal-organic framework@divinylbenzene composite monolith

Kareem Yusuf [a,*], Osama Shekhah [b], Ahmad Aqel [a], Seetah Alharbi [a], Ali S. Alghamdi [a], Reem M. Aljohani [a], Zeid A. ALOthman [a], Mohamed Eddaoudi [b]

[a] Department of Chemistry, College of Science, King Saud University, P.O. Box 2455, Riyadh, 11451, Saudi Arabia
[b] Functional Materials Design, Discovery and Development Research Group (FMD3), Advanced Membranes and Porous Materials Centre (AMPMC), Physical Sciences and Engineering Division, King Abdullah University of Science and Technology (KAUST), P.O. Box 6900, Jeddah, 23955, Saudi Arabia

ARTICLE INFO

Keywords:
Porous polymers
Gas chromatography
C_2 ternary mixture
Ethylene purification
Adsorptive separation

ABSTRACT

Ethylene is a vital intermediate in the petrochemical industry, and its purification from a C_2 ternary mixture of up to 99.9% is essential to obtain a polymer-grade gas in an energy-demanding process. Adsorption-based separation offers an alternative approach for ethylene purification in a one-step process. Here, we report the fabrication of a monolithic composite from a zeolite-like metal-organic framework with a sodalite topology (**sod**-ZMOF) incorporated into a divinylbenzene polymer (ZMOF@DVB), to purify ethylene from binary and ternary mixtures of C_2 hydrocarbons. The monolithic structure provides the composite with mechanical stability and high permeability, while only 2.31 wt% loading of **sod**-ZMOF nanoparticles has increased the BET surface area by 2.5 times, focused the pore size at 10.1 Å, and allowed for specific interactions. Gas chromatography was used to investigate the separation performance of the composite, reviling a quite satisfying selectivity of ethane/ethylene (1.89) and acetylene/ethylene (1.28), with comparable values to those of benchmark adsorbents used for similar applications and calculated via the ideal adsorbed solution theory (IAST). It is proposed that the anionic framework boosted the high polarizable ethane molecules' adsorption over ethylene; on the other hand, the Lewis basic nature of the extra-framework imidazolium cations neutralizes the anionic ZMOF structure drives acetylene's preferential adsorption over ethylene. As a proof of concept, imidazolium cations were exchanged in-situ by Na^+ cations, and selectivities decreased to 1.37 for ethane/ethylene and 1.15 for acetylene/ethylene. An inverse gas chromatography approach was utilized to evaluate the thermodynamic parameters and showed an enthalpic-entropic motivated separation before cation exchange. However, after removing bulky imidazolium cations, separation became more entropic-driven.

1. Introduction

Ethylene is a fundamental intermediate in the petrochemical industry, with a 214 million tons production capacity in 2021 [1], accounting for 0.3% of global energy consumption with propane production [2]. Ethylene is usually obtained by steam cracking and thermal decomposition of either naphtha or ethane. This process produces acetylene and ethane as downstream byproducts. Consequently, it is essential to remove acetylene and ethane from the ternary mixture in order to obtain polymer-grade ethylene with a purity of more than 99.9% [3]. Currently, ethylene purification is executed in an energy-demanding, eco-unfriendly stepwise process. Acetylene is first eliminated through catalytic hydrogenation or solvent extraction of cracked olefins using organic solvents. Afterward, ethane can be separated from ethylene by employing conventional cryogenic distillation [4]. Therefore, many research endeavors have strived for sustainable, less energy-consuming alternative approaches.

Adsorption-based industrial separation is a promising technology for demarcating the high energy consumption associated with chemical separation processes [5–8]. In this context, metal-organic frameworks (MOFs) provide an excellent adsorbent for light hydrocarbon separations due to their tunable pore size and tailor-made functionality [9–12]. Binary mixture separations of either ethane/ethylene or acetylene/-ethylene were addressed in several researches using MOFs [13–17]. In contrast, the more desirable purification of ethylene from a ternary mixture via MOFs is still scarce [18–22]. Although it is ultimately

* Corresponding author.
E-mail address: kmahmoud@ksu.edu.sa (K. Yusuf).

https://doi.org/10.1016/j.micromeso.2023.112630
Received 24 March 2023; Received in revised form 27 April 2023; Accepted 2 May 2023
Available online 3 May 2023
1387-1811/

efficient to purify ethylene from a ternary mixture in a one-step process, it is a challenging mission for a single adsorbent. The separation difficulty of the ternary mixture originates from the similarity in C_2 gases' kinetic and physicochemical properties (Table S1); ethylene properties lie between ethane and acetylene, hindering the existence of a high selectivity adsorbent.

The most common adsorption preference in MOFs is in favor of acetylene, the molecule with more π electrons and the highest quadrupole moment among the ternary mixture, followed by ethylene and then ethane. Therefore, enhancing acetylene adsorption is usually motivated by integrating highly polar moieties, such as open metal sites, or by fine-tuning pore openings [23–27]. Simultaneously, boosting acetylene adsorption will enhance ethylene adsorption over ethane. On the other hand, motivating ethane adsorption over ethylene could be achieved by utilizing nonpolar pores nature or ethane-selective sites relying on ethane's high polarizability [28–32]. Favoring ethane adsorption strategies also strengthens ethylene adsorption over acetylene.

Several studies discovered MOFs with an unintentionally higher affinity toward ethane and acetylene than ethylene without purposeful design and relatively low selectivity [33–39]. However, the persistent need has led Gu et al. to develop a strategy to fabricate MOFs specific for adsorption-based one-step ethylene purification from a ternary mixture [40]. They immobilized a Lewis basic amino group ($-NH_2$) as an acetylene affinity site into an inert pore structure ethane selective Zr-based MOF (UiO-67). The proposed strategy simultaneously boosted the selectivities of acetylene/ethylene (2.1) and ethane/ethylene (1.7) at ambient conditions, as evaluated by the ideal adsorbed solution theory (IAST). The same successful method was adopted in recent work by replacing the amino with the trifluoromethyl functionalization of UiO-66 [41]. As a result, the selectivity values of acetylene/ethylene and ethane/ethylene on UiO-66-CF_3 were estimated to be 1.4 and 1.9, respectively, allowing for one-step ethylene purification from a ternary mixture.

Recently, we have explored the light hydrocarbons separation performance of an indium-based zeolite-like metal-organic framework with a sodalite topology (**sod-**ZMOF) incorporated into divinylbenzene (DVB) monolithic composite (ZMOF@DVB). The McReynolds polarity study revealed that the nonpolar nature of the material increased with the percentage of **sod-**ZMOF in the composite [42]. Accordingly, the nonpolar nature of the material disclosed an expected ethane-affinity nature. On the other hand, the extra-framework imidazolium cations neutralize the anionic **sod-**ZMOF structure and have a strong Lewis basic character that can enhance acetylene selectivity [43–45]. Lee et al. demonstrated a higher affinity of imidazolium-based MOF (JCM-1) toward acetylene over ethylene and carbon dioxide [46]. Based on the strategy mentioned above to prepare an adsorbent to purify ethylene from a ternary mixture in a one-step process, ZMOF@DVB monolithic composite was a promising candidate with its nonpolar structure and immobilized imidazolium cations.

This work exhibits the utilization of ZMOF@DVB composite monolith to separate the ethane/ethylene binary mixture and C_2 ternary mixture with preferential adsorption of ethane and acetylene over ethylene. The composite material under study was in the form of 18 cm long × 0.25 mm internal diameter monolithic chromatographic column, and the separation efficiency was examined using a conventional gas chromatograph. The monolithic structure provides the composite with higher mechanical stability, efficient mass transfer, and high permeability [47], in addition to consuming minimal MOF material (10 mg mL^{-1}). As a proof of concept, the in-situ cationic exchange of imidazolium ions with Na^+ ions was tested to evaluate the effect of removing the Lewis base from the framework. Gas chromatography (GC) was introduced as a fast, practical alternative to simulation techniques to detect a particular guest–host preferential adsorption with comparable selectivity to that of IAST. Furthermore, thermodynamic parameters were calculated for the composite through inverse gas chromatography technique (IGC) before and after cation exchange to understand the adsorption mechanism better.

2. Experimental section

2.1. Chemicals and materials

Indium (III) nitrate hydrate, 4,5-imidazoledicarboxylaic acid (4,5-ImDC), PVP30, dimethylformamide (DMF), imidazole, and divinylbenzene (DVB) monomers were obtained from Sigma-Aldrich (St. Louis, MO, USA). Fused silica capillaries (250 μm i.d.) were purchased from CM Scientific Ltd (Bradford, UK). Azobisisobutyronitrile (AIBN) and 3-(trimethoxysilyl) propyl methacrylate (TMSM) were purchased from Fluka (Buchs, Switzerland). High-purity grade (99.9999%) gases (methane, ethane, ethylene, acetylene, helium, hydrogen, nitrogen, and air) were purchased from SIGAS (Riyadh, Saudi Arabia). Acetonitrile, dimethylformamide (DMF), 1-dodecanol, and methanol were obtained from Merck (Darmstadt, Germany). None of the compounds were further purified before usage.

2.2. Instrumentation

PXRD patterns were conducted on a D8 Advance X-ray diffractometer (Bruker, Germany) with Cu K-alpha radiation (λ = 1.5406 Å). A TA Instruments hi-res TGA Q500 thermogravimetric analyzer was employed for thermogravimetric analysis (TGA) under a constant N_2 flow and a heating rate of 278 K per minute. A Zeiss DSM 950 scanning electron microscope and an FEI QUANTA 200 3D scanning electron microscope with a tungsten filament as the electron source operating at 10 kV were used to collect the SEM pictures.

A Shimadzu 2025 Series conventional gas chromatograph was used for all chromatographic investigations. A split/splitless injection unit (SPL), an oven with a temperature range of +283–673 K and a heating rate of 287.5 K s^{-1}, and a flame ionization detector (FID) with a fuel mixture of 1:10 (hydrogen: air) are all included in the system. Samples were injected manually after the bulk temperature of the injector and detector was set to 523 K. The carrier gas was dry, high-purity (99.9999) helium.

2.3. *Sod*-ZMOF nanoparticles preparation

A 20 ml sonication vial was filled with 15 mg of $In(NO_3)_3.\ 2H_2O$ dissolved in 1 ml of DMF, 15 mg of 4,5-ImDC dissolved in acetonitrile, 0.2 ml of 1.47 M imidazole DMF solution, and 0.5 ml of 0.01 M PVP30 in DMF. During 24 h, the mixture was heated at 358 K while stirring. The item was thoroughly washed with DMF three times before being solvent exchanged with methanol every 12 h for two days.

2.4. Monolithic composite preparation

The monolithic material preparation method was tuned to provide a high permeability with relatively large pores [48]. In order to immobilize the monolithic bed inside the capillary columns, pretreatment of the inner wall was performed before polymerization. A two meter empty tubing (250 μm i.d) was flushed with 1.0 mol L^{-1} NaOH solution, distilled water, 0.2 mol L^{-1} HCl, distilled water again, and then with acetone for 30 min each, followed by drying under a nitrogen stream for 2 h. The capillary tubing was then filled with 40 wt% acetone solution of 3-(trimethoxysilyl) propyl methacrylate (TMSM) and left to stand for 2 h, rinsed with acetone, and dried for 2 h using N_2. A syringe pump was utilized in all flushing steps under a flow rate of 20 μL min^{-1}.

A polymerization mixture was then prepared in a 2 ml vial with 42.3 wt% of divinylbenzene, and 57.7 wt% of 1-dodecanol and toluene binary porogen, 52.3 wt% and 5.4 wt%, respectively, in addition to 1 wt% Azobisisobutyronitrile (AIBN) initiator, then sonicated for 10 min and purged with helium for 10 min. Only 18 cm out of 30 cm of the capillary's middle part was filled with polymerization mixture by hanging the

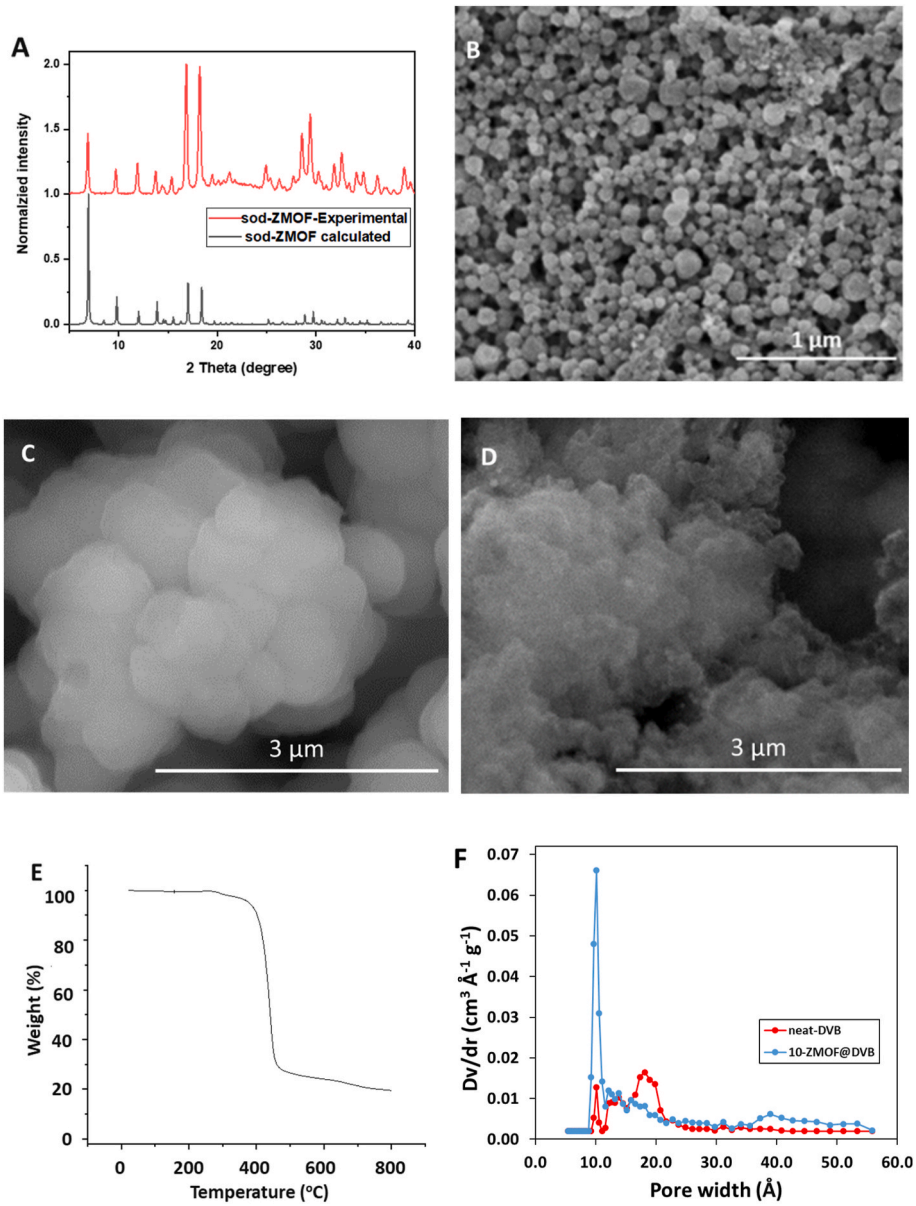

Fig. 1. Characterization of **sod**-ZMOF nanoparticles, neat-DVB, and 10-ZMOF@DVB. (A) PXRD pattern of **sod**-ZMOF nanoparticles compared with its simulation pattern. (B, C, and D) SEM images of **sod**-ZMOF nanoparticles, neat-DVB monolith, and 10-ZMOF@DVB monolithic composite, respectively. (E) TGA curve of the 10-ZMOF@DVB. (F) Pore size distributions calculated via DFT method for neat-DVB and 10-ZMOF@DVB monoliths.

column in a U-shape to avoid continuously exposing the polymerized monolith to the gas chromatograph's inlet and outlet high temperature (523 K). After adding the polymerization mixture to the pretreated capillary tubing and capping it with GC septa, thermal polymerization was conducted inside the GC oven at 346 K for 30 min for the columns and the remaining solution in the vials for characterization.

In addition to the blank polymer column batch (neat-DVB), another batch incorporated with 10 mg mL^{-1} **sod**-ZMOF (10-ZMOF@DVB) was also prepared. A post-polymerization washing step was conducted overnight under a constant flow of methanol using an HPLC pump, flushing out the unreacted molecules and residual solvents. Next, all the prepared columns were preconditioned, firstly under a constant temperature of 313 K and a pressure up to 10 bar with an increasing rate of 0.1 bar min^{-1}, secondly under a constant pressure of 5 bar and a temperature program starting with 313 K (10 min) up to 523 K (30 min) with a ramp rate of 276 K min^{-1}. Finally, bulk monolithic samples were thoroughly washed with methanol for 12 h using Soxhlet extraction and then dried at 333 K for 2 h before being used for characterization.

All the working columns, whether neat-DVB or 10-ZMOF@DVB, underwent an in-situ cationic exchange procedure using Na^{+} solution to evaluate the cation exchange effect on separation efficiency without affecting the material's morphological characters. A 1 mmol L^{-1} NaCl in 95% aqueous methanol solution was used to wash the columns under a constant flow of 0.03 mL min^{-1} for 24 h, followed by 3 h of washing with pure methanol under the same flow rate.

2.5. Chromatographic conditions and calculations

Gas-tight syringes were used in all chromatographic experiments, and the flow rates (F_a) were determined via a soap bubble method using a 100 µL pipette. Methane gas was considered an unretained probe to determine the dead time (t_0) under experimental conditions. Permeability (K^o) of the monolithic composites was estimated by the modified Darcy's law [49]:

$$K^{\circ} = \frac{u\eta L}{\Delta P\, j'} \quad (1)$$

Where u is the carrier gas velocity and η is its viscosity, L is the column length, ΔP is the column inlet minus outlet pressure, and j′ is the Halasz compressibility correlation factor:

$$j' = \frac{3(P^2-1)(P+1)}{4(P^3-1)}, \text{ where P equals } P_i \Big/ P_o \quad (2)$$

The average channels diameter (R) of the monolithic material was determined using Hagen–Poiseuille equation [50]:

$$u = \frac{\Delta P R^2}{8\eta L} \quad (3)$$

The separation performance of ethane, ethylene, and acetylene using the prepared monolithic columns was evaluated by calculating separation selectivity and resolution, where selectivity (α) is the stationary phase chromatographic differentiation ability between two probes:

$$\alpha = \frac{t_{R2} - t_0}{t_{R1} - t_0} \quad (4)$$

Where t_R is the retention time, and t_0 is the dead time.

And resolution (R_S) describes the degree of separation between successive peaks:

$$R_S = 1.18\, \frac{t_{R2} - t_{R1}}{w_{(0.5)1} + w_{(0.5)2}} \quad (5)$$

Where $w_{(0.5)}$ is the peak width at half height.

2.6. Physicochemical calculations

A specific retention volume (V_g) is considered equivalent to the inflection point in breakthrough studies [51,52], and it was the basic value to calculate all of the thermodynamic parameters at infinite dilution and the range 313–333 K under 5 bar using equation (6):

$$V_g = 3 \Big/ 2 \left[\frac{273.15\,(t_R - t_m)F_a\, j}{w\, T}\right] \quad (6)$$

Where T and w are the working temperature and the weight of the stationary phase, respectively, while j is the James-Martin gas compressibility factor which is calculated as follows:

$$j = \frac{3(P^2-1)}{2(P^3-1)} \quad (7)$$

as P is the ratio between the column and outlet pressure [53].

The enthalpy change of adsorption (ΔH_A) can be estimated by plotting the logarithm of the specific retention volume versus the inverse of absolute temperature. The adsorption enthalpy change represents the adsorbate–adsorbent interaction strength at zero surface coverage:

$$\Delta H_A = -R\, \frac{d \ln V_g}{d\,(1/T)} \quad (8)$$

The standard free energy change of adsorption (ΔG_A) is determined using equation (9) [54]:

$$\Delta G_A = -RT \ln\left(\frac{V_g P^{\circ}}{S\, \pi_0}\right) \quad (9)$$

Where S is the specific surface area of the adsorbent, the reference two-dimensional surface pressure is represented by π_0, and P° is the vapor pressure of the adsorbate, which can be estimated using Antoine's equation:

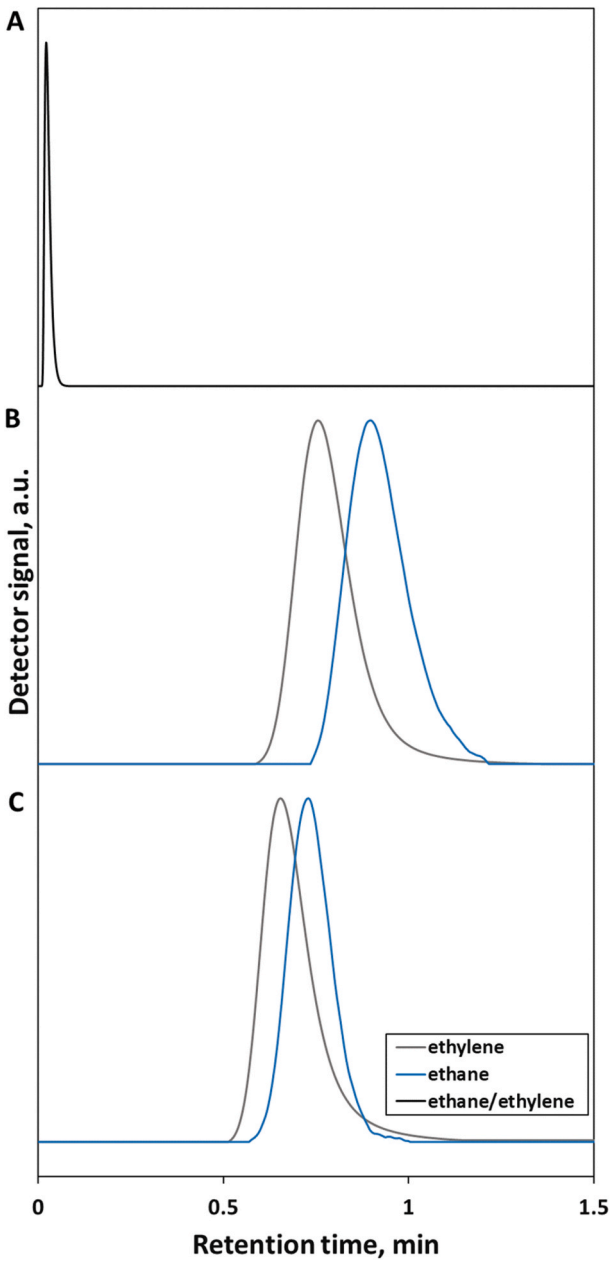

Fig. 2. Gas chromatograms of ethane/ethylene binary mixture separations at 323 K, using (A) neat-DVB column, (B) 10-ZMOF@DVB column, and (C) 10-ZMOF@DVB-Na column (18 cm long × 0.25 mm inner diameter). The injection volume was 4 μL, and the data was recorded at 5 bar constant helium pressure.

$$\text{Log}\,(P^{\circ}) = A - \left(\frac{B}{t + C}\right) \quad (10)$$

Where A, B, and C are the Antoine coefficients [55], and t is the working temperature in Celsius.

The standard entropy change of adsorption (ΔS_A) is calculated at zero surface coverage using equation (11):

$$\Delta S_A = \frac{\Delta H_A - \Delta G_A}{T} \quad (11)$$

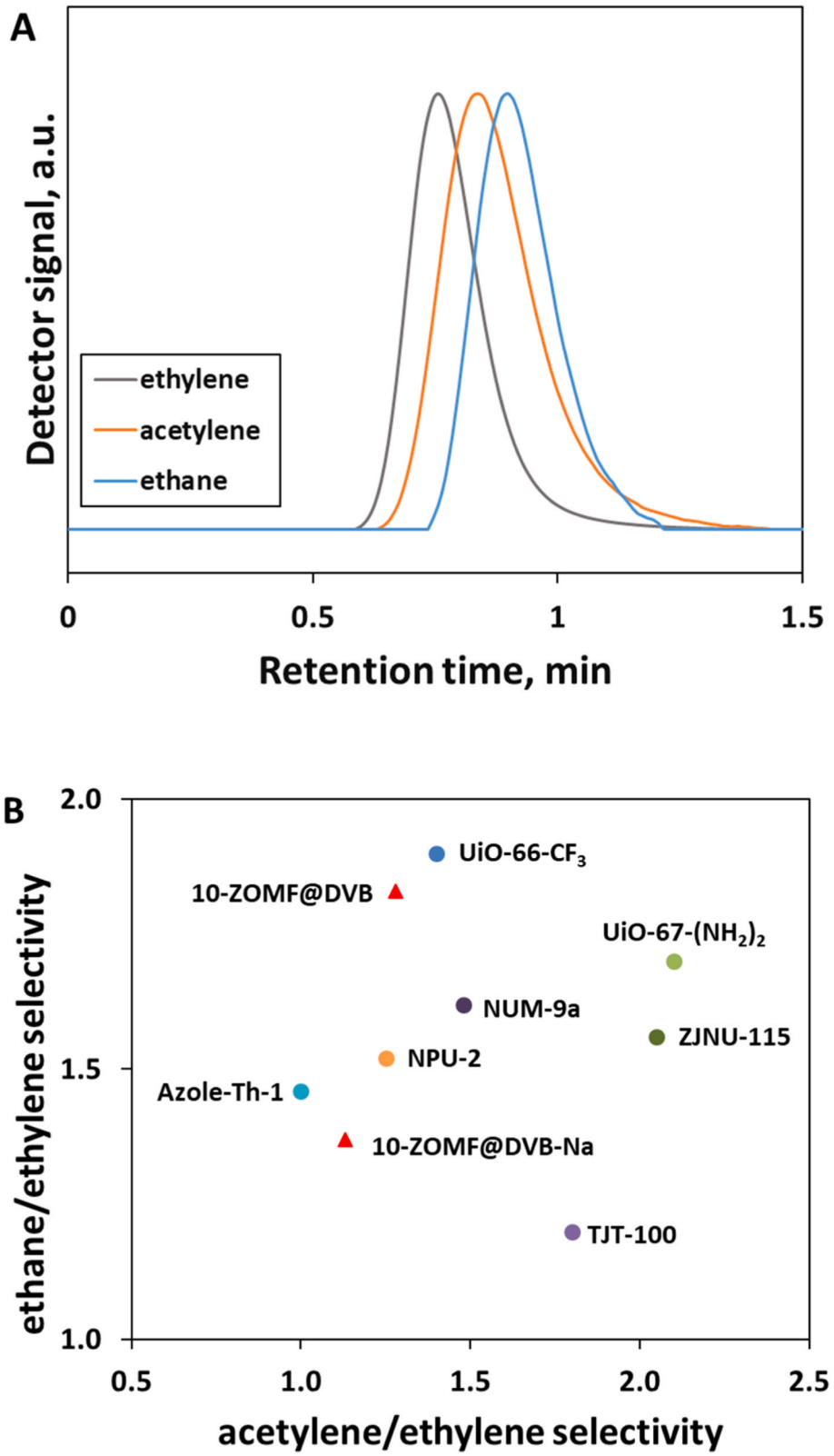

Fig. 3. Ethane/acetylene/ethylene ternary mixture. (A) Gas chromatogram at 323 K, using 10-ZMOF@DVB column (18 cm long × 0.25 mm inner diameter), injection volume 4 μL and the data was recorded at 5 bar constant helium pressure. (B) Chromatographic selectivity comparison of 10-ZMOF@DVB with reported adsorbents based on IAST selectivity at ambient conditions.

3. Discussion

3.1. Characterization of *sod*-ZMOF and ZMOF@DVB composite

The phase purity of **sod**-ZMOF was verified with PXRD, and a very good concordance between the calculated and as-synthesized **sod**-ZMOF patterns was confirmed (Fig. 1A). In addition, a nano-size of 200 nm was estimated for **sod**-ZMOF particles via SEM, showing no aggregates (Fig. 1B). The neat-DVB monolith's SEM results revealed well-developed macropores with an average diameter of 5–10 μm surrounding medium size microglobules with a diameter range of 1–2 μm (Fig. 1C). In contrast, adding 2.31 wt% **sod**-ZMOF nanoparticles to the monolithic structure had a deforming effect and formed smaller clusters (Fig. 1D).

Nitrogen adsorption-desorption experiments were performed to characterize the neat-DVB monolith and the 10-ZMOF@DVB monolithic composite (Fig. S1). The BET surface area increased 2.5 times from 99.24 $m^2\ g^{-1}$ in the neat-DVB to 243.76 $m^2\ g^{-1}$ in 10-ZMOF@DVB monolithic composite by incorporating only 10 mg mL^{-1} **sod**-ZMOF of the total polymerization mixture. In addition, the fabricated composite showed excellent thermal stability up to 250 °C (Fig. 1E). The average nano-pores sizes of the neat-DVB monolith calculated by the nonlocal density functional theory (DFT) were distributed between 12.1 and 23.8 Å (Fig. 1F). In contrast, for 10-ZMOF@DVB, pore size was concentrated at 10.1 Å, demonstrating the effect of ZMOF incorporation in decreasing the average nano-pore size, bringing a closer adsorbate–adsorbent contact.

3.2. Separation of C_2 hydrocarbon mixture

Preferential ethane adsorption over ethylene using 10-ZMOF@DVB monolithic composite immobilized inside a capillary column (18 cm long × 0.25 mm i.d.) was confirmed by a gas chromatographic separation. However, no separation was detected using the neat-DVB monolith for the 50/50 ethane/ethylene binary mixture with a retention time similar to the dead time of methane, indicating no retention for either gas (Fig. 2A). While the incorporation of 2.31 wt% **sod**-ZMOF nanoparticles into the DVB monolithic matrix dramatically boosts the adsorption behavior of the material with a selectivity equal to 1.89 toward ethane over ethylene and a resolution of 1.14 at 323 K, claiming a complete separation (Fig. 2B and Table S2). We believe that the primary motivation for the preferential adsorption of ethane is its higher polarizability than ethylene, boosting the favorable interactions with the anionic framework and its hosted imidazolium cations [56]. On the other hand, Lewis basic imidazolium cations also promote the adsorption of the more acidic ethylene molecules [40].

To verify this hypothesis, the 10-ZMOF@DVB composite monolith was utilized to separate a ternary mixture of ethane, ethylene, and acetylene with the ratio 1:1:1 (Fig. 3A). The location of the acetylene peak after ethylene (acetylene/ethylene selectivity = 1.28) but before ethane (ethane/acetylene selectivity = 1.44) proved the effect of imidazolium basicity on the highest acidity acetylene molecules (pKa = 26). Obviously, the polarizability effect still drives ethane adsorption to outweigh acidity-driven acetylene adsorption.

Further proof of concept was demonstrated through a cation exchange of the Lewis base imidazolium ions with Na^+ ions in-situ to form a 10-ZMOF@DVB-Na, as described in the experimental section, to examine the effect of removing imidazolium cations on ethane/ethylene separation while keeping the same monolithic structure. Furthermore, a similar Na^+ cation exchange procedure was performed on the neat-DVB column to detect the effect of the exchange process on the DVB structure and composition. Carrier gas permeability across the monolithic skeleton of the neat-DVB monolith and the average channel diameter did not change before and after the cation exchange procedure, $104 \times 10^{-13}\ m^2$ and 7.99 μm, respectively, indicating no effect of Na^+ cation exchange on either monolithic structure or DVB composition. Successful cation exchange was indicated by a permeability elevation of the 10-ZMOF@DVB-Na monolith to $8.52 \times 10^{-13}\ m^2$ from $6.87 \times 10^{-13}\ m^2$ in ZMOF@DVB monolith, and the average channel diameter increased from 2.05 μm to 2.28 μm, as a result of replacing the bulky imidazolium cations with Na^+ cations. A lower selectivity (1.37) and lower resolution (0.54) in terms of chromatographic separation of ethane/ethylene binary mixture were detected when using 10-ZMOF@DVB-Na monolith at 323 K, revealing the case of decreasing separation efficiency after excluding the Lewis basic imidazolium cations out of ZMOF structure (Fig. 2C and Table S2). In the case of ternary mixture separation on the 10-ZMOF@DVB-Na monolith, acetylene separated from ethylene and still adsorbed favorably but with a lower acetylene/ethylene selectivity (1.15) may be due to the incomplete removal of imidazolium during the in-situ cation exchange.

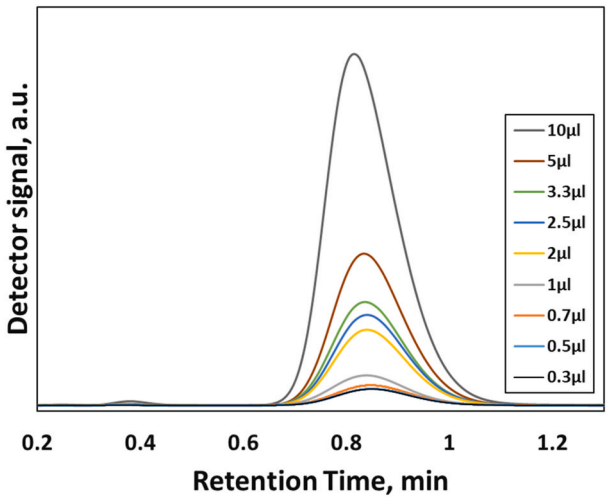

Fig. 4. A typical GC chromatogram of ethane adsorption/desorption on 10-ZMOF@DVB over a range of sample sizes at 323 K. Data recorded at 5 bar.

The genuine work of Pires et al. on ethane/ethylene separation using IRMOF-8 reasonably compared chromatographic selectivity with IAST selectivity [57]. Accordingly, the comparison of this work's selectivities with the benchmark adsorbents that are able to purify ethylene in a one-step process showed that 10-ZMOF@DVB has a remarkable performance at ambient temperature conditions and even at higher pressure (Fig. 3B) [40,41,58–62]. It can be concluded that the effect of imidazolium polarizability on ethane molecules with higher polarizability, in addition to the anionic framework effect, had a decisive influence in favoring ethane adsorption on ZMOF@DVB composite monolith. In contrast, the Lewis basic nature of imidazolium drives acetylene's preferential adsorption over ethylene.

3.3. Thermodynamic calculation

In order to gain a deeper understanding of the preferential adsorption of acetylene and ethane over ethylene on 10-ZMOF@DVB, thermodynamic parameters were estimated via inverse gas chromatography (IGC) study and compared to those of 10-ZMOF@DVB-Na in the range 313–333 K and under a constant pressure of 5 bar. The retention volumes of the probe molecules at infinite dilution (Henry's region) are used to calculate thermodynamic quantities. At Henry's region, the surface coverage unaffected the uptake, and the molecules interact solely with high-energy sites. The zero coverage region of ethane on 10-ZMOF@DVB was studied and confirmed (Fig. 4). Each peak in Fig. 4 represents a different ratio of surface coverage, and the peak area or height is directly proportional to the number of molecules received by the detector. As injection volume increases, there is a deviation from Henry's law and less symmetry of the chromatogram. However, for injection volumes between 0.3 and 10 μL, there is no significant shift in retention times with an RSD% of 5%, with perfect symmetry over the

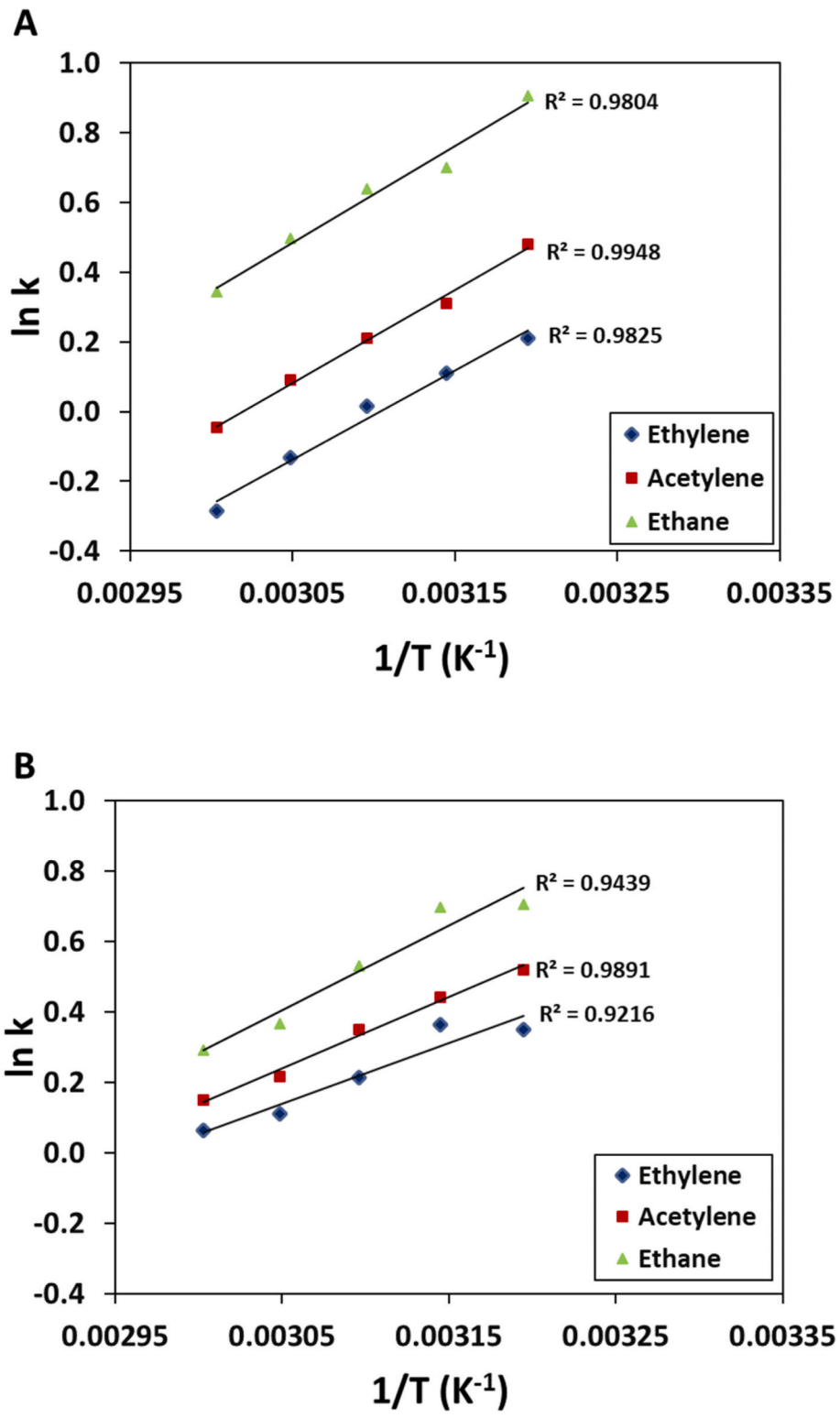

Fig. 5. Van't Hoff plots of ethylene, acetylene, and ethane, respectively, according to their elution order, on 10-ZMOF@DVB and 10-ZMOF@DVB-Na columns in the range 313–333 K. Data recorded at 5 bar.

range. Accordingly, 4 μL was chosen as the experimental injection volume throughout the present work to ensure working at Henry's region.

A linear relationship of Van't Hoff plots suggested that the interaction mechanism had not changed throughout the experimental temperature range (Fig. 5). The spontaneous transfer of test probes between the stationary phase and carrier gas was demonstrated by the negative values of the Gibbs free energy of adsorption (ΔG_A) (Table S5). Adsorption enthalpies (ΔH_A) were calculated using the slope of plots of $\ln V_g$ versus 1/T (Fig. S2). This linear dependency suggests that ΔH_A is constant over the investigated temperature range. Adsorbate-adsorbent interactions overwhelmed adsorbate–adsorbate interactions, indicated by a higher enthalpy of adsorption values than the enthalpy of liquefaction (ΔH_{liq}) for the studied materials (Table 1) [63]. The closeness between ΔH_A and ΔH_{liq} values revealed domination of the van der Waals

Table 1
Entropy change of adsorption (ΔS_A) at 323 K, the enthalpy change of adsorption (ΔH_A) at the range 313–333 K, and enthalpy of liquefaction (ΔH_{liq}), of ethylene, acetylene, and ethane, respectively, according to their elution order, on 10-ZMOF@DVB (ZMOF) and 10-ZMOF@DVB-Na (ZNOF-Na) columns. Data recorded at 5 bar.

Probes	$-\Delta S_A$ (J mol^{-1} K^{-1})		$-\Delta H_A$ (kJ mol^{-1})		$-\Delta H_{liq}$ (kJ mol^{-1})
	ZMOF	ZMOF-Na	ZMOF	ZMOF-Na	
ethylene	25.59	13.67	29.51	25.82	14.0
acetylene	28.49	22.16	30.36	28.31	16.3
ethane	29.46	32.58	31.27	31.61	15.3

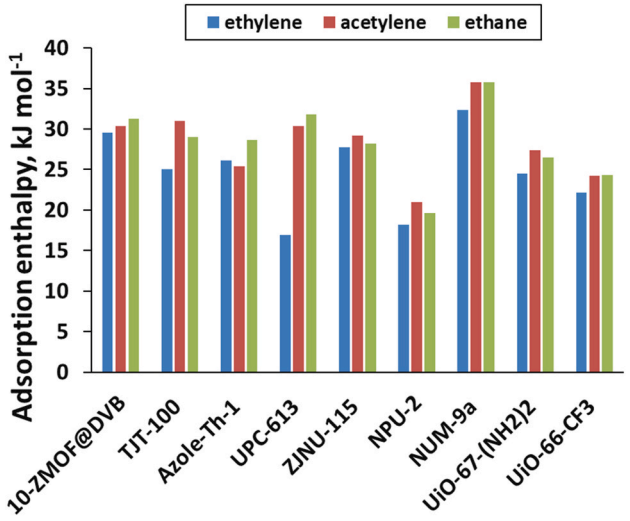

Fig. 6. Enthalpy of adsorption comparison of 10-ZMOF@DVB with reported adsorbents able to separate ethane/acetylene/ethylene ternary mixture.

forces-driven interactions, demonstrating energetically homogeneous interaction surfaces. It is worth noting that the calculated absolute values of ΔH_A of C_2 adsorption on 10-ZMOF@DVB and 10-ZMOF@DVB-Na were comparable to the isosteric heat of adsorption (differential enthalpy of adsorption) (Q_{st}) estimated using the virial equation or the Clausius-Clapeyron equation at zero coverage from benchmark work on adsorption based one-step purification of ethylene from C_2 ternary mixture (Fig. 6 and Table S6).

As expected, the enthalpy of ethane adsorption on 10-ZMOF@DVB was the highest (31.27 kJ mol^{-1}), followed by that of acetylene (30.36 kJ mol^{-1}), and finally, the ethylene value (29.51 kJ mol^{-1}), in agreement with chromatogram's elution order (Fig. 3A). Similarly, the entropy of adsorption values (ΔS_A) confirmed the stabilization of ethane molecules throughout the material down to ethylene with the highest degree of freedom and the lowest adsorption and demonstrated enthalpic-entropic motivated adsorption (table 1, S7). After exchanging the imidazolium cations with Na^+ cations, ΔH_A of ethane slightly increased, while ΔS_A values increased significantly, indicating changing the adsorption mechanism to become more entropic driven. This could be due to the increasing ability of ethane molecules approaching the anionic framework and to make use of its higher hydrogen content and free rotation around the single bond to build more C–H … π and C–H•••N interactions, and hence more stabilization. On the contrary, ΔH_A and ΔS_A values of acetylene and ethylene adsorption on 10-ZMOF@DVB-Na were markedly decreased without changing the fact that ethylene has the lowest adsorbability as a result of an incomplete in-situ exchange of the Lewis basic imidazolium residues.

4. Conclusions

In conclusion, the chromatographic selectivity and the thermodynamic study confirmed the applicability of ZMOF@DVB monolithic composite for the one-step ethylene purification from a C_2 binary and ternary mixture using only 2.31 wt% as-synthesized **sod**-ZMOF. The anionic nonpolar nature of ZMOF brought a high affinity toward ethane molecules with the highest polarizability among the ternary mixture. At the same time, the extra-framework imidazolium Lewis bases boosted the adsorption capacity of acidic acetylene molecules. Furthermore, we anticipate that ZMOF@DVB monolithic composite can be used to purify ethylene from a quaternary mixture as ZMOF has a high affinity toward CO_2, as confirmed in our previous study because it has similar characteristics of ethane in terms of high polarizability [64].

Future work could focus on optimizing the composite's performance by tuning the framework's anionic nature and exploring different ZMOF topologies. Additionally, utilizing various heterocyclic compounds with higher Lewis basicity to exchange imidazolium cations could enhance ethylene purification further. Finally, the proposed MOF@Polymer composite presents a promising solution for ethylene purification taking advantage of monolithic structure scalability, cost-effectiveness, high mechanical stability, and permeability, in addition to MOFs tunability, high surface area, and tailor-made functionality. Exploring the composite's stability under different operating conditions and scaling up the synthesis process could be potential areas of future research.

CRediT authorship contribution statement

Kareem Yusuf: Writing – review & editing, Writing – original draft, Software, Methodology, Data curation, Conceptualization. **Osama Shekhah:** Writing – original draft, Methodology, Conceptualization. **Ahmad Aqel:** Validation, Software. **Seetah Alharbi:** Methodology. **Ali S. Alghamdi:** Methodology. **Reem M. Aljohani:** Visualization, Methodology. **Zeid A. AlOthman:** Supervision. **Mohamed Eddaoudi:** Supervision.

Declaration of competing interest

The authors declare the following financial interests/personal relationships which may be considered as potential competing interests: Kareem Yusuf reports financial support was provided by the National Plan of Science, Technology and Innovation (MAARIFAH), King Abdulaziz City for Science and Technology, Kingdom of Saudi Arabia, grant number 14-ADV2447-02.

Data availability

Data will be made available on request.

Acknowledgments

This work was supported through the project funded by the National Plan of Science, Technology and Innovation (MAARIFAH), King Abdulaziz City for Science and Technology, Kingdom of Saudi Arabia, grant number 14-ADV2447-02.

Appendix A. Supplementary data

Supplementary data to this article can be found online at https://doi.org/10.1016/j.micromeso.2023.112630.

References

[1] Ethylene production capacity globally, Statista, 2021 (n.d.), https://www.statista.com/statistics/1067372/global-ethylene-production-capacity/. (Accessed 22 February 2023).

[2] D.S. Sholl, R.P. Lively, Seven chemical separations to change the world, Nat 532 (2016) 435–437, https://doi.org/10.1038/532435a, 2016 5327600.

[3] S. Chu, Y. Cui, N. Liu, The path towards sustainable energy, Nat. Mater. 161 (2017) 16–22, https://doi.org/10.1038/nmat4834, 16 (2016.

[4] S.M. Sadrameli, Thermal/catalytic cracking of liquid hydrocarbons for the production of olefins: a state-of-the-art review II: catalytic cracking review, Fuel 173 (2016) 285–297, https://doi.org/10.1016/J.FUEL.2016.01.047.

[5] K. Yusuf, A. Aqel, Z. Alothman, Metal-organic frameworks in chromatography, J. Chromatogr. A 1348 (2014) 1–16, https://doi.org/10.1016/j.chroma.2014.04.095.

[6] X. Li, Y. Liu, J. Wang, J. Gascon, J. Li, B. Van Der Bruggen, Metal–organic frameworks based membranes for liquid separation, Chem. Soc. Rev. 46 (2017) 7124–7144, https://doi.org/10.1039/C7CS00575J.

[7] Y. Cheng, S.J. Datta, S. Zhou, J. Jia, O. Shekhah, M. Eddaoudi, Advances in metal–organic framework-based membranes, Chem. Soc. Rev. 51 (2022) 8300–8350, https://doi.org/10.1039/D2CS00031H.

[8] D.S. Bell, The current status of metal-organic frameworks (MOFs) for use in liquid chromatography, LC-GC North Am 40 (2022) 63–65, https://doi.org/10.56530/LCGC.NA.KT3688W6.

[9] H. Furukawa, K.E. Cordova, M. O'Keeffe, O.M. Yaghi, The chemistry and applications of metal-organic frameworks, Science 80– (2013) 341, https://doi.org/10.1126/SCIENCE.1230444/SUPPL_FILE/FURUKAWA.SM.CORRECTED.PDF.

[10] T. Islamoglu, S. Goswami, Z. Li, A.J. Howarth, O.K. Farha, J.T. Hupp, Postsynthetic tuning of metal-organic frameworks for targeted applications, Acc. Chem. Res. 50 (2017) 805–813, https://doi.org/10.1021/ACS.ACCOUNTS.6B00577/ASSET/IMAGES/LARGE/AR-2016-00577A_0009. JPEG.

[11] H. Wang, Y. Liu, J. Li, H. Wang, J. Li, Y. Liu, Designer metal–organic frameworks for size-exclusion-based hydrocarbon separations: progress and challenges, Adv. Mater. 32 (2020), 2002603, https://doi.org/10.1002/ADMA.202002603.

[12] W.G. Cui, T.L. Hu, X.H. Bu, Metal-organic framework materials for the separation and purification of light hydrocarbons, Adv. Mater. 32 (2020), https://doi.org/10.1002/ADMA.201806445.

[13] J. Wang, L. Li, L. Guo, Y. Zhao, D. Xie, Z. Zhang, Q. Yang, Y. Yang, Z. Bao, Q. Ren, Adsorptive separation of acetylene from ethylene in isostructural Gallate-based metal–organic frameworks, Chem. Eur J. 25 (2019) 15516–15524, https://doi.org/10.1002/CHEM.201903952.

[14] Z. Zhang, S. Bo Peh, Y. Wang, C. Kang, W. Fan, D. Zhao, Z. Zhang, S.B. Peh, Y. Wang, C. Kang, W. Fan, D. Zhao, Efficient trapping of trace acetylene from ethylene in an ultramicroporous metal–organic framework: synergistic effect of high-density open metal and electronegative sites, Angew. Chem. Int. Ed. 59 (2020) 18927–18932, https://doi.org/10.1002/ANIE.202009446.

[15] H. Li, C. Liu, C. Chen, Z. Di, D. Yuan, J. Pang, W. Wei, M. Wu, M. Hong, An unprecedented pillar-cage fluorinated hybrid porous framework with highly efficient acetylene storage and separation, Angew. Chem. Int. Ed. 60 (2021) 7547–7552, https://doi.org/10.1002/ANIE.202013988.

[16] G.D. Wang, R. Krishna, Y.Z. Li, W.J. Shi, L. Hou, Y.Y. Wang, Z. Zhu, Boosting ethane/ethylene separation by MOFs through the amino-functionalization of pores, Angew. Chem. Int. Ed. 61 (2022), e202213015, https://doi.org/10.1002/ANIE.202213015.

[17] F. Anwar, M. Khaleel, K. Wang, G.N. Karanikolos, Selectivity tuning of adsorbents for ethane/ethylene separation: a review, Ind. Eng. Chem. Res. 2022 (2022) 12269–12293, https://doi.org/10.1021/ACS.IECR.2C02438/ASSET/IMAGES/LARGE/IE2C02438_0017 (JPEG).

[18] H.G. Hao, Y.F. Zhao, D.M. Chen, J.M. Yu, K. Tan, S. Ma, Y. Chabal, Z.M. Zhang, J. M. Dou, Z.H. Xiao, G. Day, H.C. Zhou, T.B. Lu, Simultaneous trapping of C2H2 and C2H6 from a ternary mixture of C2H2/C2H4/C2H6 in a robust metal–organic framework for the purification of C2H4, Angew. Chem. Int. Ed. 57 (2018) 16067–16071, https://doi.org/10.1002/ANIE.201809884.

[19] Y. Wang, C. Hao, W. Fan, M. Fu, X. Wang, Z. Wang, L. Zhu, Y. Li, X. Lu, F. Dai, Z. Kang, R. Wang, W. Guo, S. Hu, D. Sun, One-step ethylene purification from an acetylene/ethylene/ethane ternary mixture by cyclopentadiene cobalt-functionalized metal–organic frameworks, Angew. Chem. Int. Ed. 60 (2021) 11350–11358, https://doi.org/10.1002/ANIE.202100782.

[20] G.D. Wang, Y.Z. Li, W.J. Shi, L. Hou, Y.Y. Wang, Z. Zhu, One-step C2H4 purification from ternary C2H6/C2H4/C2H2 mixtures by a robust metal–organic framework with customized pore environment, Angew. Chem. Int. Ed. 61 (2022), e202205427, https://doi.org/10.1002/ANIE.202205427.

[21] X.W. Gu, J.X. Wang, E. Wu, H. Wu, W. Zhou, G. Qian, B. Chen, B. Li, Immobilization of Lewis basic sites into a stable ethane-selective MOF enabling one-step separation of ethylene from a ternary mixture, J. Am. Chem. Soc. 144 (2022) 2614–2623, https://doi.org/10.1021/JACS.1C10973/ASSET/IMAGES/LARGE/JA1C10973_0004. JPEG.

[22] Yunjia Jiang, Yongqi Hu, Binquan Luan, Lingyao Wang, Rajamani Krishna, Haofei Ni, X. Hu, Y. Zhang, Benchmark single-step ethylene purification from ternary mixtures by a customized fluorinated anion-embedded MOF, Nat. Commun. 141 (2023) 14, https://doi.org/10.1038/s41467-023-35984-5, 2023) 1–9.

[23] J. Pei, K. Shao, J.X. Wang, H.M. Wen, Y. Yang, Y. Cui, R. Krishna, B. Li, G. Qian, A chemically stable hofmann-type Metal−Organic framework with sandwich-like binding sites for benchmark acetylene capture, Adv. Mater. 32 (2020), 1908275, https://doi.org/10.1002/ADMA.201908275.

[24] Y.Y. Xue, X.Y. Bai, J. Zhang, Y. Wang, S.N. Li, Y.C. Jiang, M.C. Hu, Q.G. Zhai, Precise pore space partitions combined with high-density hydrogen-bonding acceptors within metal–organic frameworks for highly efficient acetylene storage and separation, Angew. Chem. Int. Ed. 60 (2021) 10122–10128, https://doi.org/10.1002/ANIE.202015861.

[25] X. Jiang, T. Pham, J.W. Cao, K.A. Forrest, H. Wang, J. Chen, Q.Y. Zhang, K.J. Chen, Molecular sieving of acetylene from ethylene in a rigid ultra-microporous metal organic framework, Chem. Eur J. 27 (2021) 9446–9453, https://doi.org/10.1002/CHEM.202101060.

[26] S.Q. Yang, L. Zhou, Y. He, R. Krishna, Q. Zhang, Y.F. An, B. Xing, Y.H. Zhang, T. L. Hu, Two-dimensional metal-organic framework with ultrahigh water stability for separation of acetylene from carbon dioxide and ethylene, ACS Appl. Mater. Interfaces 14 (2022) 33429–33437, https://doi.org/10.1021/ACSAMI.2C09917/SUPPL_FILE/AM2C09917_SI_002.CIF.

[27] F. Zheng, R. Chen, Y. Liu, Q. Yang, Z. Zhang, Y. Yang, Q. Ren, Z. Bao, F. Zheng, R. Chen, Y. Liu, Q. Yang, Z. Zhang, Y. Yang, Q. Ren, Z. Bao, Strengthening intraframework interaction within flexible MOFs demonstrates simultaneous sieving acetylene from ethylene and carbon dioxide, Adv. Sci. (2023), 2207127, https://doi.org/10.1002/ADVS.202207127.

[28] C. Gücüyener, J. Van Den Bergh, J. Gascon, F. Kapteijn, Ethane/ethene separation turned on its head: selective ethane adsorption on the metal-organic framework ZIF-7 through a gate-opening mechanism, J. Am. Chem. Soc. 132 (2010) 17704–17706, https://doi.org/10.1021/JA1089765/SUPPL_FILE/JA1089765_SI_001.PDF.

[29] L. Li, R.B. Lin, R. Krishna, H. Li, S. Xiang, H. Wu, J. Li, W. Zhou, B. Chen, Ethane/ethylene separation in a metal-organic framework with iron-peroxo sites, Science 80– (2018) 443–446, https://doi.org/10.1126/SCIENCE.AAT0586/SUPPL_FILE/AAT0586-LI-SM.PDF, 362.

[30] H. Yang, Y. Wang, R. Krishna, X. Jia, Y. Wang, A.N. Hong, C. Dang, H.E. Castillo, X. Bu, P. Feng, Pore-space-Partition-enabled exceptional ethane uptake and ethane-selective ethane-ethylene separation, J. Am. Chem. Soc. 142 (2020) 2222–2227, https://doi.org/10.1021/JACS.9B12924/SUPPL_FILE/JA9B12924_SI_002.CIF.

[31] K. Su, W. Wang, S. Du, C. Ji, D. Yuan, Efficient ethylene purification by a robust ethane-trapping porous organic cage, Nat. Commun. 121 (2021) 1–7, https://doi.org/10.1038/s41467-021-24042-7, 12 (2021.

[32] S. Geng, E. Lin, X. Li, W. Liu, T. Wang, Z. Wang, D. Sensharma, S. Darwish, Y. H. Andaloussi, T. Pham, P. Cheng, M.J. Zaworotko, Y. Chen, Z. Zhang, Scalable room-temperature synthesis of highly robust ethane-selective metal-organic frameworks for efficient ethylene purification, J. Am. Chem. Soc. 143 (2021) 8654–8660, https://doi.org/10.1021/JACS.1C02108/SUPPL_FILE/JA1C02108_SI_005.CIF.

[33] H.G. Hao, Y.F. Zhao, D.M. Chen, J.M. Yu, K. Tan, S. Ma, Y. Chabal, Z.M. Zhang, J. M. Dou, Z.H. Xiao, G. Day, H.C. Zhou, T.B. Lu, Simultaneous trapping of C2H2 and C2H6 from a ternary mixture of C2H2/C2H4/C2H6 in a robust metal–organic framework for the purification of C2H4, Angew. Chem. Int. Ed. 57 (2018) 16067–16071, https://doi.org/10.1002/ANIE.201809884.

[34] Z. Xu, X. Xiong, J. Xiong, R. Krishna, L. Li, Y. Fan, F. Luo, B. Chen, A robust Th-azole framework for highly efficient purification of C2H4 from a C2H4/C2H2/C2H6 mixture, Nat. Commun. 111 (2020) 1–9, https://doi.org/10.1038/s41467-020-16960-9, 11 (2020.

[35] S.Q. Yang, F.Z. Sun, P. Liu, L. Li, R. Krishna, Y.H. Zhang, Q. Li, L. Zhou, T.L. Hu, Efficient purification of ethylene from C2 hydrocarbons with an C2H6/C2H2-selective metal-organic framework, ACS Appl. Mater. Interfaces 13 (2021) 962–969, https://doi.org/10.1021/ACSAMI.0C20000/SUPPL_FILE/AM0C20000_SI_002.CIF.

[36] Y. Wang, C. Hao, W. Fan, M. Fu, X. Wang, Z. Wang, L. Zhu, Y. Li, X. Lu, F. Dai, Z. Kang, R. Wang, W. Guo, S. Hu, D. Sun, One-step ethylene purification from an acetylene/ethylene/ethane ternary mixture by cyclopentadiene cobalt-functionalized metal–organic frameworks, Angew. Chem. Int. Ed. 60 (2021) 11350–11358, https://doi.org/10.1002/ANIE.202100782.

[37] B. Zhu, J.W. Cao, S. Mukherjee, T. Pham, T. Zhang, T. Wang, X. Jiang, K.A. Forrest, M.J. Zaworotko, K.J. Chen, Pore engineering for one-step ethylene purification from a three-component hydrocarbon mixture, J. Am. Chem. Soc. 143 (2021) 1485–1492, https://doi.org/10.1021/JACS.0C11247/ASSET/IMAGES/LARGE/JA0C11247_0004. JPEG.

[38] R.E. Sikma, N. Katyal, S.K. Lee, J.W. Fryer, C.G. Romero, S.K. Emslie, E.L. Taylor, V.M. Lynch, J.S. Chang, G. Henkelman, S.M. Humphrey, Low-valent metal ions as MOF pillars: a New route toward stable and multifunctional MOFs, J. Am. Chem. Soc. 143 (2021) 13710–13720, https://doi.org/10.1021/JACS.1C05564/SUPPL_FILE/JA1C05564_SI_001.PDF.

[39] Y. Liu, H. Xiong, J. Chen, S. Chen, Z. Zhou, Z. Zeng, S. Deng, J. Wang, One-step ethylene separation from ternary C2 hydrocarbon mixture with a robust zirconium metal–organic framework, Chin. J. Chem. Eng. (2023), https://doi.org/10.1016/J.CJCHE.2023.01.001.

[40] X.W. Gu, J.X. Wang, E. Wu, H. Wu, W. Zhou, G. Qian, B. Chen, B. Li, Immobilization of Lewis basic sites into a stable ethane-selective MOF enabling one-step separation of ethylene from a ternary mixture, J. Am. Chem. Soc. 144 (2022) 2614–2623, https://doi.org/10.1021/JACS.1C10973/SUPPL_FILE/JA1C10973_SI_001.PDF.

[41] J. Liu, J. Miao, H. Wang, Y. Gai, J. Li, Enhanced one-step purification of C2H4 from C2H2/C2H4/C2H6 mixtures by fluorinated Zr-MOF, AIChE J. (2023), e18021, https://doi.org/10.1002/AIC.18021.

[42] K. Yusuf, O. Shekhah, A. Aqel, S. Alharbi, A.S. Alghamdi, R.M. Aljohani, M. Eddaoudi, Z.A. Alothman, A monolithic composite based on zeolite-like metal-organic framework@divinylbenzene polymer separates azeotropic fluorocarbon mixture efficiently, J. Chromatogr. A 1694 (2023), 463922, https://doi.org/10.1016/J.CHROMA.2023.463922.

[43] Y. Liu, V.C. Kravtsov, R. Larsen, M. Eddaoudi, Molecular building blocks approach to the assembly of zeolite-like metal–organic frameworks (ZMOFs) with extra-large cavities, Chem. Commun. (2006) 1488–1490, https://doi.org/10.1039/B600188M.

[44] B. Demir, M.G. Ahunbay, CO2/CH4 separation in ion-exchanged zeolite-like metal organic frameworks with sodalite topology (sod-ZMOFs), J. Phys. Chem. C 117 (2013) 15647–15658, https://doi.org/10.1021/JP4033657/SUPPL_FILE/JP4033657_SI_001.PDF.

[45] B.A. Al-Maythalony, O. Shekhah, R. Swaidan, Y. Belmabkhout, I. Pinnau, M. Eddaoudi, Quest for anionic MOF membranes: continuous sod -ZMOF membrane with Co2 adsorption-driven selectivity, J. Am. Chem. Soc. 137 (2015) 1754–1757, https://doi.org/10.1021/JA511495J/SUPPL_FILE/JA511495J_SI_001.PDF.

[46] J. Lee, C.Y. Chuah, J. Kim, Y. Kim, N. Ko, Y. Seo, K. Kim, T.H. Bae, E. Lee, Separation of acetylene from carbon dioxide and ethylene by a water-stable microporous metal–organic framework with aligned imidazolium groups inside the channels, Angew. Chem. Int. Ed. 57 (2018) 7869–7873, https://doi.org/10.1002/ANIE.201804442.

[47] R. Seabra, V.F.D. Martins, A.M. Ribeiro, A.E. Rodrigues, A.P. Ferreira, Ethylene/ethane separation by gas-phase SMB in binderfree zeolite 13X monoliths, Chem. Eng. Sci. 229 (2021), 116006, https://doi.org/10.1016/J.CES.2020.116006.

[48] D. Peroni, R.J. Vonk, W. van Egmond, H.G. Janssen, Macroporous polymer monoliths as second dimension columns in comprehensive two-dimensional gas chromatography: a feasibility study, J. Chromatogr. A 1268 (2012) 139–149, https://doi.org/10.1016/J.CHROMA.2012.10.019.

[49] F. Svec, A.A. Kurganov, Less common applications of monoliths: III. Gas chromatography, J. Chromatogr. A 1184 (2008) 281–295, https://doi.org/10.1016/J.CHROMA.2007.07.014.

[50] M. Zabka, M. Minceva, A.E. Rodrigues, Experimental characterization and modelling of analytical monolithic column, J. Biochem. Biophys. Methods 70 (2007) 95–105, https://doi.org/10.1016/J.JBBM.2006.10.002.

[51] S. Mohammadi-Jam, K.E. Waters, Inverse gas chromatography applications: a review, Adv. Colloid Interface Sci. 212 (2014) 21–44, https://doi.org/10.1016/j.cis.2014.07.002.

[52] P.P. Ylä-Mäihäniemi, D.R. Williams, A comparison of frontal and nonfrontal methods for determining solid-liquid adsorption isotherms using inverse liquid chromatography, Langmuir 23 (2007) 4095–4101, https://doi.org/10.1021/la0632631.

[53] A.T. James, A.J. Martin, Gas-liquid partition chromatography; the separation and micro-estimation of volatile fatty acids from formic acid to dodecanoic acid, Biochem. J. 50 (1952) 679–690, https://doi.org/10.1042/bj0500679.

[54] L. Lavielle, J. Schultz, Surface properties of carbon fibers determined by inverse gas chromatography: role of pretreatment, Langmuir 7 (1991) 978–981, https://doi.org/10.1021/la00053a027.

[55] I. Smallwood, Handbook of Organic Solvent Properties, first ed., Butterworth-Heinemann, 1996 (accessed March 6, 2023), http://www.sciencedirect.com:5070/book/9780080523781/handbook-of-organic-solvent-properties?via=ihub=.

[56] B.A. Al-Maythalony, O. Shekhah, R. Swaidan, Y. Belmabkhout, I. Pinnau, M. Eddaoudi, Quest for anionic MOF membranes: continuous sod -ZMOF membrane with Co2 adsorption-driven selectivity, J. Am. Chem. Soc. 137 (2015) 1754–1757, https://doi.org/10.1021/JA511495J/SUPPL_FILE/JA511495J_SI_001.PDF.

[57] J. Pires, M.L. Pinto, V.K. Saini, Ethane selective IRMOF-8 and its significance in ethane-ethylene separation by adsorption, ACS Appl. Mater. Interfaces 6 (2014) 12093–12099, https://doi.org/10.1021/AM502686G/SUPPL_FILE/AM502686G_SI_001.PDF.

[58] H.G. Hao, Y.F. Zhao, D.M. Chen, J.M. Yu, K. Tan, S. Ma, Y. Chabal, Z.M. Zhang, J. M. Dou, Z.H. Xiao, G. Day, H.C. Zhou, T.B. Lu, Simultaneous trapping of C2H2 and C2H6 from a ternary mixture of C2H2/C2H4/C2H6 in a robust metal–organic framework for the purification of C2H4, Angew. Chem. Int. Ed. 57 (2018) 16067–16071, https://doi.org/10.1002/ANIE.201809884.

[59] Z. Xu, X. Xiong, J. Xiong, R. Krishna, L. Li, Y. Fan, F. Luo, B. Chen, A robust Th-azole framework for highly efficient purification of C2H4 from a C2H4/C2H2/C2H6 mixture, Nat. Commun 111 (11) (2020) 1–9, https://doi.org/10.1038/s41467-020-16960-9.

[60] B. Zhu, J.W. Cao, S. Mukherjee, T. Pham, T. Zhang, T. Wang, X. Jiang, K.A. Forrest, M.J. Zaworotko, K.J. Chen, Pore engineering for one-step ethylene purification from a three-component hydrocarbon mixture, J. Am. Chem. Soc. 143 (2021) 1485–1492, https://doi.org/10.1021/JACS.0C11247/ASSET/IMAGES/LARGE/JA0C11247_0004. JPEG.

[61] S.Q. Yang, F.Z. Sun, P. Liu, L. Li, R. Krishna, Y.H. Zhang, Q. Li, L. Zhou, T.L. Hu, Efficient purification of ethylene from C2 hydrocarbons with an C2H6/C2H2-selective metal-organic framework, ACS Appl. Mater. Interfaces 13 (2021) 962–969, https://doi.org/10.1021/ACSAMI.0C20000/SUPPL_FILE/AM0C20000_SI_002.CIF.

[62] L. Fan, P. Zhou, X. Wang, L. Yue, L. Li, Y. He, Rational construction and performance regulation of an in(III)-Tetraisophthalate framework for one-step adsorption-phase purification of C2H4from C2Hydrocarbons, Inorg. Chem. 60 (2021) 10819–10829, https://doi.org/10.1021/ACS.INORGCHEM.1C01560/SUPPL_FILE/IC1C01560_SI_001.PDF.

[63] D.W.H. Rankin, in: David R. Lide (Ed.), CRC Handbook of Chemistry and Physics, 89th edition, 2009, pp. 223–224, https://doi.org/10.1080/08893110902764125, 10.1080/08893110902764125. 15.

[64] B.A. Al-Maythalony, O. Shekhah, R. Swaidan, Y. Belmabkhout, I. Pinnau, M. Eddaoudi, Quest for anionic MOF membranes: continuous sod -ZMOF membrane with Co2 adsorption-driven selectivity, J. Am. Chem. Soc. 137 (2015) 1754–1757, https://doi.org/10.1021/JA511495J/SUPPL_FILE/JA511495J_SI_001.PDF.